Engineering Structures, Volume 28, Issue 12, , October 2006, Pages 1671-1690

Investigations with a bandwidth measure for fatigue assessment of the Foinaven dynamic umbilical including VIV

F. Trarieux*[1], G. J. Lyons**, M. H. Patel*

*School of Engineering, Cranfield University, Cranfield, Bedfordshire MK43 0AL, UK

**BPP Technical Services Ltd., Dilke House, 1 Malet Street, London WC1E 7JN, UK

Abstract

An innovative use of a method to detect Vortex Induced Vibration (VIV) bandwidth in the curvature data of subsea flexible risers and umbilicals is presented. The parameter epsilon gives a valuable estimate of the bandwidth of signals such as VIV as a single value which may be used to track the behaviour with time and against other measures such as current speed. The method is conveniently based on a peak counting approach originally used in a marine context by Cartwright and Longuet-Higgins. Low epsilon values close to zero indicate a narrow band process whereas values near unity indicate a broad-band process. Curvature and environmental data were gathered by the Foinaven Umbilical Monitoring System (FUMS) installed on the Foinaven Petrojarl IV floating production unit located in the Altantic margin, west of Shetland. The VIV frequency range owing to current excitation considered is that in the range 0.2 to 2Hz. This paper presents analyses showing the correlation of the epsilon bandwidth parameter with standard deviation of curvature, current speed and spectral analysis results for extended periods measured on the Foinaven dynamic umbilical. Examination of the number of frequencies and their values using spectrograms over long periods enable interesting interpretation of the build up and decay of the VIV behaviour. These data are also reduced to the predominant peak frequencies, and standard deviation along with epsilon to provide a compact description of the VIV behaviour over 10 minute intervals. Clear frequency and amplitude shifts can be observed as VIV varies with currents ebb and flow. The behaviour is usefully described using only epsilon, standard deviation, and peak frequencies. The importance of epsilon for fatigue damage assessment is demonstrated through a formulation derived by Wirsching & Light. Strong VIV regimes are often characterized by an intense activity around a particular frequency and the impact of such relatively narrow-band events on the fatigue life of the structure is clearly demonstrated. This paper also presents the relative contributions of mooring, and waves/vessel motions, and VIV to fatigue damage. Although wave excitation remains the main source of fatigue, VIV appears to potentially contribute to a significant part of the overall fatigue damage.

Keywords: Vortex Induced Vibration, VIV, bandwidth, epsilon, FUMS, fatigue, rainflow counting

[1] Corresponding author: Tel: +44 (0) 1234 754-603, Fax: +44 (0) 1234 758-230, Email: f.trarieux@cranfield.ac.uk

1. Introduction

Vortex Induced Vibration (VIV) continues to be a source of major concern in the offshore industry, particularly with risers and umbilicals. The accurate prediction of response e.g. Lyons (1986a) proves to be rather difficult for realistic applications owing to the complexities of geometry and environmental loading. Given this, it is preferable not to rely upon prediction alone, but also to monitor the behaviour in the installed condition. By this means it is possible potentially to take corrective action in advance of likely (fatigue) failure, and also to improve our understanding of the shortcomings of the predictions made.

Part of the complexity of VIV response is as a consequence of marine riser and umbilical systems' ability to respond simultaneously to several modes of vibration. The extent to which this may happen is described as response bandwidth. Plainly it is of interest to measure this frequency response as well as having basic information concerning amplitude. Whilst it is possible to perform spectral analyses, this approach arguably provides too much information for routine consideration. It is possible to apply System Identification techniques to characterize the spectra, Mandal et al. (1992). However, a single-value measure of bandwidth variation with time (and varying environmental loading) is highly desirable. This paper presents a measure for this purpose which has existed for some time. We refer to this as epsilon. This has been demonstrated by the authors to be a better measure than kurtosis which was suggested by Vandiver (2000). Kurtosis is a measure of how outlier-prone the data are, and as such is a measure of how steady the amplitude is. In certain circumstances steady amplitude may equate to a steady frequency indicating narrow-bandedness – but this is not generally so.

Application of the epsilon technique is demonstrated with data from the Foinaven Umbilical Monitoring System (FUMS) for which a wide range of VIV and environmental loading data is available. This system was developed and installed and is maintained by BPP Technical Services on the BP Foinaven Petrojarl IV FPSO in the Atlantic Frontier West of Shetland province of the UK. It was designed to measure (for the life of the field) the curvature in the umbilical, along with vessel motions and environmental data. These data combined with current profiles enable effective analysis of the dynamic response of the umbilical.

In the method presented, curvature time series are processed so as to identify the occurrence of VIV using the bandwidth parameter epsilon. This very usefully has a range between 0 and 1 depending on the frequency content of the signal (narrow or broad-band process).

Nomenclature

a, b	empirical constants
D	fatigue damage
$E[D_{NB}]$	mean or expected value of D for narrow-band stress
D_{RFC}	value of D using a rainflow counting technique
D_{ε}	value of D using epsilon based formulation
FUMS	Foinaven Umbilical Monitoring System
K	empirical constant in S-N curve
m	slope of S-N curve
N	cycles to failure
N_0^+	number of zero crossings with (+) slope
N_1	total number of maxima
n_{RFC}	number of rainflow cycles in a record
n	total number of cycles in a record
n_i^+	number of up-crossings in record i
$P(\kappa)$	probability distribution function of maxima of curvature
S	random variable denoting stress cycle
$\overline{S^m}$	mean value of S^m
sde	standard deviation
T	fatigue life (time to failure)
T_{rec}	record duration
VIV	Vortex Induced Vibration
ε	bandwidth parameter
λ	correction factor function of m and ε
σ	root-mean-square of bending stress
υ_0^+	expected rate of zero crossings with (+) slope
$\Gamma(\cdot)$	gamma function

2. Bandwidth parameter epsilon

The basis for the technique presented is that developed by Longuet-Higgins (1952), and Cartwright and Longuet-Higgins (1956) who carried out substantial work on the distribution of maxima of random functions to investigate the distribution of wave heights and ship motions. This followed the early work by Rice (1944, 1945) on random noise. Extension to consideration for VIV analysis was first reported for experimental and theoretical VIV data by Lyons (1986b).

The random function may be defined as the sum of an infinite number of sine waves :

$$f(t) = \sum_{n} c_n \cos(f_n t + \varphi_n) \tag{1}$$

with:

f_n : frequency in the interval $[0, \infty]$,

φ_n : random phase in the interval $[0, 2\pi]$.

The amplitude c_n is such that in any small interval of frequency df : $\sum_{f_n = f}^{f+df} \frac{1}{2} c_n^2 = E(f)df$

Where $E(f)$ is a continuous function of f called the energy spectrum of $f(t)$. It is noted here that the expression given in Eq. (1) is not the exact definition of a random function, since there should be a condition of randomness for the amplitude c_n, as was reported by Tucker et al. (1984).

Cartwright and Longuet-Higgins originally used the joint probability distribution function of the maxima of a random function where epsilon appears as a measure of the rms width of the energy spectrum. The formulation of epsilon then depends on the moments (m_n) of the energy spectrum:

$$\varepsilon = \sqrt{\left(\frac{m_0 m_4 - m_2^2}{m_0 m_4} \right)} \tag{2}$$

with:

$$m_n = \int_0^{\infty} E(f) f^n df \tag{3}$$

They showed that epsilon could be based on the proportion of negative maxima to total maxima:

$$\varepsilon^2 = 1 - (1 - 2r)^2 \tag{4}$$

with:

$$r = \frac{1}{2}(1 - \frac{N_0^+}{N_1}) \tag{5}$$

r : proportion of negative maxima

N_0^+ : number of up-crossing periods

N_1 : total number of maxima

The definitions of positive maxima, positive minima, negative maxima, negative minima, zero up-crossing, zero down-crossing are shown in Fig. 1.

From Eqs. (4) and (5) we obtain:

$$\varepsilon = \sqrt{1 - \left(\frac{N_0^+}{N_1}\right)^2} \tag{6}$$

Epsilon is conveniently seen to depend only on the number of zero up-crossings and on the number of maxima in the signal. It is this approach that has been applied as presented herein. The ratio $\left(N_0^+ / N_1\right)$ has been termed the 'irregularity factor' by some authors e.g. Lalane (2002), Barltrop and Adams (1991). Epsilon is used by ourselves since it is a more sensitive measure than the irregularity factor as the bandwidth becomes narrower.

2.1 Peak distribution and epsilon

The following demonstrates graphically why the peak counting approach is appropriate. The frequency content of a signal has a direct influence on the peak distribution. For example consider a simple combination of three sinusoidal signals of different frequencies (0.05, 0.5, and 5 Hz as shown in Fig. 2). In these it is seen that the number of zero up-crossings reduces drastically compared to the number of maxima as more frequencies are present in the signal.

According to Eq. (4), if we consider an infinite number of sinusoids, the ratio $\left(N_0^+ / N_1\right) \to 0$ and then $\varepsilon \to 1$ (i.e. epsilon tends to unity for broad-band signals). Considering the case of a narrow-band signal, for a single sinusoidal signal the ratio $\left(N_0^+ / N_1\right) \to 1$ and then $\varepsilon \to 0$ (i.e. epsilon tends to zero for narrow-band signals).

3. The Foinaven Umbilical Monitoring System (FUMS)

The system was installed in 1996 on the Floating Production Storage and Offloading vessel (FPSO) *'Petrojarl IV'* on the Foinaven Field located west of Shetlands in 465 metres water depth, Lyons et al. (1998, 2003). The system uses a specially developed curvature sensor, which is deployed in a spare $^{5}/_{8}$ inch hydraulic control hose in the umbilical. The umbilical is of a lazy-wave configuration, Fig. 3.

The sensor measures curvature at three locations noted L1, L2, L3, in horizontal plane orthogonal (X and Y) directions in the region of the umbilical bend stiffener, Fig. 4. It is terminated at the FPSO connector deck level and extends through the vessel depth to the measurement region below the vessel keel.

Curvature is detected using strain gauges configured in pairs for each location and direction to ensure tension and temperature effects are eliminated, and resultant curvature and plane are calculated. The main processing unit samples 16 channels of analogue data at 20 samples/sec/channel, for a total of 8192 samples per channel. Hence each sampling period is just under 7 minutes. The 20 Hz sampling rate was chosen to deal with anticipated 3Hz vortex induced vibration frequencies. The 7 minute sampling period being sufficiently adequate to cope with a few cycles of FPSO mooring system long period surge and sway.

Signals for environmental (wave statistics) and vessel motions are also read and stored as part of the FUMS data set. Additionally detailed current data through the water column are separately available at 10 minute intervals measured using Acoustic Doppler Current Profiling.

Subsequent to acquisition the FUMS data are processed which includes marking for quality, filtering, calculation of statistical values (minimum, maximum, mean, standard deviation, kurtosis), incrementation of fatigue cycle counting rainflow tables, and storage of time series data if defined criteria have been met. Where time series data have been retained it has been possible to carry out further analysis (epsilon, kurtosis, and spectral).

4. Analysis of curvature data

4.1 Raw Data Filtering

The raw curvature data contain all the components of curvature owing to the wave excitation, surface vessel motion and VIV. In order to examine only the VIV components in the curvature signal, the raw data were band-pass filtered between 0.2 and 10 Hz. This was further split into two ranges of 0.2 to 2 Hz and 2 to 10 Hz. The 2 to 10 Hz range contains little data of interest, as a consequence the range 0.2 to 2Hz is

presented. A potential source of contamination of the filtered curvature signal in the range [0.2 – 2 Hz] might be due to the overlap between the proper VIV components and the waves and vessel motions components. It was considered that wave and vessel motion responses would not be significant below 4 seconds period (0.25 Hz). The filter used allows for imperfect sharpness. Plainly it is possible that some VIV response may exist in the region below 0.2 Hz. Evidence from the variation in umbilical dynamic response with current indicated that this is probably not generally significant, Lyons et al (2003). Trarieux (2004) demonstrated that for some environmental circumstances this behaviour would be expected to occur, according to the authors' own VIV prediction tool – VIVALL- Fang and Lyons (1991).

4.2 Epsilon analysis

Whereas kurtosis has been adopted since 2000 as a standard statistical measure as part of the FUMS statistical analysis at the time of data acquisition, epsilon has yet to be implemented in this way. Consequently it has only been possible to perform the epsilon analysis on data that have been retained as time series. It should be noted that statistical data (measured at 7 minute intervals) are retained at all times by FUMS, but time series data are generally discarded unless certain pre-set criteria are met.

The epsilon analysis was implemented in FORTRAN code processing sequentially the daily records during the period considered. For the year 2000 period analysis presented herein, 16 records of 7 minutes each were available from 16 June to 12 July providing a total of nearly 2 hours every day. For the year 2001 period analysis also presented herein, 64 records of 7 minutes each were available from 25-Jan-01 to 19-Apr-01 providing a total of nearly 7.5 hours every day.

4.3 Variation of bandwidth with amplitude and current

Figs. 5a,b show for the VIV components the results of the epsilon analysis compared with standard deviation of curvature as well as current data for the period 16-Jun-00 to 12-Jul-00. Fig. 5a presents the results for the X component and Fig. 5b the Y component. These are shown in accumulated form such that there is a spread of 16 consecutive values clustered about each day for each measurand. Current profiles were recorded between 64 and 400 metres water depth. The current speeds presented in Figs. 5a and 5b are records at 64 metres depth.

A close match between epsilon, amplitude (standard deviation of curvature), and the current speed can be clearly seen. For greater clarity, 1-epsilon has been plotted in order to have this and amplitude and current speed varying in the same sense. There is a trend towards narrow-band response as the amplitude of VIV increases (with increasing current). The match with standard deviation of curvature can be explained

by the fact that more energy is contained in the curvature signal as the current increases. This can be observed for both X and Y components which indicates that the umbilical vibrates in both planes (in-plane and out-of-plane). It is noted however that due to an orientation error of the sensors which occurred during the installation of the FUMS it is likely that the sensors are measuring curvature in planes which are not exactly in-plane and normal-to-plane of the umbilical. The current profile although not presented here (data not available for this day) is (as is generally the case for the currents at Foinaven) unlikely to be uniform (in speed or direction) and for this reason it is expected that the VIV response is seen in both X and Y senses.

4.4 Power spectral density peaks, frequencies, and epsilon

Figs 6a,b show the results of the epsilon analysis compared with standard deviation of curvature and frequencies of spectral density peaks for 6-Feb-01 for the X and Y VIV components. This acquisition period has been chosen to demonstrate clearly the variations as the current peaks and reduces. (This is by implication since current records were not available for this period, but is consistent with all other observations – e.g. Fig 5).

In this particular case the X component is seen to exhibit more bandwidth variation than the Y component.

Fig. 7 shows the spectral analysis for selected records on 6-Feb-01. There is a clear steady shifting in frequency between record no.1 and no. 48 where the curvature becomes more narrow-banded (with increase in current speed). The peak frequency shift range is from 0.25 to 0.75 Hz.

The signal measured for the Y component shows greater differences in the psd records (see Fig. 7 record no. 64 in particular) where the level of psd becomes significantly higher than for the X component. This difference is most likely a consequence of continued change in current direction once the peak in current speed has been reached (and the tide turns) leading more favourable conditions for Y sense VIV excitation.

Fig. 8 shows the filtered curvature time series for these specific records and confirms the trend towards narrow-bandedness of the curvature at record no. 48 for which epsilon has a value of 0.54.

4.5 Power spectral density peaks, frequencies, epsilon, and current

VIV data from 20-Feb-01 are presented where the current data cover a half tide cycle from maximum to minimum current speed in order to examine the effect of significant current speed variation. The daily data acquisition was limited to 7 hours and 42 minutes between 00:00 to 07:42 am.

Figs. 9a,b show the same types of plots as Fig. 6a,b but with the current speed at 74m (current speed was not available for 6-Feb-01). The speed is reasonably steady for the first half of the acquisition period and increases steadily with a small reduction at the end. The responses in this case are similar for both X and Y components. At the start of data acquisition, the current is at its lowest value and epsilon has a value of about 0.9 (broad-band). As current speed increases, epsilon drops and reaches a minimum value of about 0.65 (more narrow-banded). As the current increases, the standard deviation also increases and the distinct peak frequencies excited are of higher order as shown on Fig. 9a (c) and Fig. 9b (c) for record nos. 49 up to 64.

The spectral analysis on Fig. 10 shows again a high peak for the Y component for record nos. 60 and 64. This is similar to 6-Feb-01, and is again believed to be as a consequence of the tide turning with flow components becoming more favourable to induce higher levels of VIV for the Y component from the changed direction.

The general trend that appears from Figs. 6a,b and 9a,b is that not only higher order modes are being excited but also a greater number of distinct modes is excited as the current speed increases. The VIV regime has been characterized in previous studies (Lyons, 1986a) sometimes by strong activity around a particular frequency. This is apparent in this study shown by the spectral analysis in Fig. 10, which shows the lower amplitudes of the distinct secondary peaks.

Fig. 11 presents the results of the bandwidth analysis for an extended period between 10-Feb-01 and 18-Apr-01. The consistency of the epsilon analysis is demonstrated here where the current peaks are well matched with epsilon and otherwise by amplitude of curvature (as standard deviation). It can be seen that as the current increases, a greater number of distinct frequencies is present in the curvature signal as shown on Fig. 11d. This may seem to be in contradiction with epsilon having a low value (indicating a narrow-band process). There are two main considerations which might be applied here. The first is to assume that as the current increases, higher order modes are excited and also that a greater number of modes is present in the signal. In this sense the response would be considered more broad-band when the current increases. The other consideration (which is confirmed in this study) is that higher order modes are excited and that only one or two distinct modes are predominant so the response becomes narrow-banded as the current increases. Results from spectral analysis and analysis of the time-series confirm the narrow-band characteristic of the curvature response for higher current speed (in the case of this umbilical). The secondary distinct peaks shown in Fig. 10d (which are unnoticeable apart from the second peak) have relatively low amplitudes compared to the main peak at around 0.5 Hz.

4.5.1 Skewness

Fig. 12 shows the variation of skewness of VIV components of curvature for the period 25-Jan-01 to 18-Apr-01 where it exhibits values between –3 and +3. Fig. 13 shows the correlation between skewness and epsilon for this period. It can be seen that when epsilon is low, skewness is very close to zero which is consistent given the narrow-band characteristic of the signal for low epsilon values. When the signal becomes broad-banded the curvature response exhibits a range of distributions in addition to normally distributed behaviour as skewness departs significantly from zero. This is understood to be as a consequence of different modes having generally different mean values. There are several factors that can explain such behaviour. Firstly, the form of the umbilical (lazy-wave) as opposed to a simple straight cylinder (such as a vertical tensioned riser) leads to much more complex (interesting) mode shapes. These may be biased by the quasi-static profile of the lazy-wave umbilical. Secondly, the slight orientation error of the monitoring sensors (referred to in Section 4.3) also has an effect. It is evident from the calculation of skewness for the VIV behaviour for this umbilical that intense VIV response (for high current speeds) is generally characterized by a predominant frequency and associated curvature amplitude response which is normally distributed. Skewness provides a useful tool to confirm the nature of the VIV response from a distribution point of view. Yu et al. (2004) discuss the importance of skewness for VIV fatigue damage assessment which is covered in the next section.

4.6 Fatigue and epsilon

Whilst it is of interest to know the displacement amplitudes which might be predicted from VIV assessment tools for subsea flexibles (risers, umbilicals, power cables, tethers) the ability to assess the level of fatigue is generally of greater importance. This capability needs to be available for a range of structural configurations (tensioned vertical, catenary, lazy-wave, steep-S, etc.) and for various current profiles which may be quite different depending on the field location (strong sheared currents through water column west of Shetland; Loop and Eddy currents in the Gulf of Mexico, for example). The range of VIV displacement amplitudes can vary widely owing to the time-varying build-up and decay of this phenomenon (as a consequence of daily, and longer term, variations in current, wave influence, inter-modal beating etc.).

As an engineering assessment tool it is noted that DnV rules for risers (2001) suggest the use of epsilon for wide-band fatigue damage assessment with principal application to direct response to wave and LF (mooring system low frequency) action. This approach may also be used for VIV. Reference to the use of epsilon as a correction factor to a narrow-band 'equivalent' response for a broad-band fatigue damage

formulation was first proposed by Wirsching and Light (1980), following the work by Miles (1954), and Crandall et al (1962). Results based on the formulation of Wirsching and Light are demonstrated herein.

4.6.1 Rainflow counting, and epsilon based fatigue assessment methods

The fatigue behaviour of the umbilical armour layers can be described using an S-N curve which is assumed to be of the form:

$$NS^m = K \tag{7}$$

where: S is the stress level i.e. range (double amplitude), N is the number of cycles to failure (for a given stress level), and K and m are empirical constants obtained from fatigue experiments (m is the slope of the S-N curve).

The fatigue damage is defined as the ratio of the number of stress cycles in a particular record to the number of stress cycles leading to failure:

$$D = \frac{n}{N} \tag{8}$$

With reference to rainflow counting methods, e.g. Matsuishi (1968):

$$D_{RFC} = \frac{n}{K}\overline{S^m} \tag{9}$$

Fatigue failure occurs if $D_{RFC} \geq 1$

Assuming Miner's rule is applicable, the estimate of $\overline{S^m}$ for n_{RFC} rainflow stress cycles is:

$$\overline{S^m} = \frac{1}{n_{RFC}}\sum_{j=1}^{n} S_j^m \tag{10}$$

Wirsching and Light (1980) proposed a formulation equivalent to a rainflow counting approach using a narrow-band approximation, D_ε:

$$D_\varepsilon = E[D_{NB}(T_{rec})]\,\lambda(m,\varepsilon) \tag{11}$$

Where $E[D_{NB}(T_{rec})]$ is the mean or expected fatigue damage for a record of duration T_{rec} for a stationary Gaussian narrow-band process:

.

$$E[D_{NB}(T_{rec})] = \frac{\upsilon_0^+ T_{rec}}{K}(\sqrt{2}\,\sigma)^m \Gamma\left(\frac{m}{2}+1\right) \tag{12}$$

Crandall et al (1962) and Lin (1967) attribute the original derivation of (12) to Miles (1954).

Eq. (12) assumes that the total number of peaks is almost the same as the number of zero crossings with positive slopes. λ is a correction factor dependent on ε which takes account of the bandwidth of the signal, modifying for the broad band case, the narrow-band case of Eq. (12). λ is defined by Wirsching and Light (1980) as:

$$\lambda(m,\varepsilon) = a(m) + \left[1 - a(m)\right](1-\varepsilon)^{b(m)} \tag{13}$$

Where:

$$a(m) = 0.926 - 0.033m \tag{14}$$

$$b(m) = 1.587m - 2.323 \tag{15}$$

a and b have been obtained experimentally and applied by Wirsching and Light (1980) for four rather varied 'typical' spectra. They used these to describe fatigue stresses in joints of offshore structures subject to wave action. A sample function was generated from the spectra using digital simulation. The rainflow cycles were identified and λ was computed for each sample using $D = \lambda\, D_{NB}$ for values of $m = 3, 4, 5, 6, 10$. The procedure was repeated 20 times in order to reduce the variance of λ. Plots of λ versus ε for given m were then obtained. Eq. (13) is a least squares curve approximation based on those plots.

Wirsching and Light (1980) proposed a variation of Eq. (12) (which includes an additional factor of 2 to account for stress range) for the case of fatigue under broad-band stresses assuming that a narrow-band fatigue stress having the same standard deviation as a broad-band fatigue stress was an accurate fatigue damage estimate. This formulation can be used as an assessment tool to determine the fatigue life T of a structure:

$$E[D_{NB}(T)] = \left(\frac{\upsilon_0^+ T}{K}\right)(2\sqrt{2}\,\sigma)^m \Gamma\left(\frac{m}{2}+1\right) \tag{16}$$

From the analysis of N_{rec} records, one can obtain an estimate of υ_0^+ and σ:

$$\upsilon_0^+ \; ; \; \frac{1}{N_{rec}} \sum_{i=1}^{N_{rec}} \frac{n_i^+}{T_i} \tag{17}$$

$$\sigma \; ; \; \frac{1}{N_{rec}} \sum_{i=1}^{N_{rec}} \sigma_i \tag{18}$$

With:

n_i^+ : number of up-crossings in record i

T_i : duration of record i (second)

N_{rec} : number of records

σ_i : standard deviation of record i

4.6.2 Comparison between epsilon based fatigue method and rainflow counting approach

The fatigue damage estimates included herein have been non-dimensionalised for presentation purposes, each has the range 0 to 1.

Fig 14 shows the variation of epsilon, epsilon based fatigue damage, and rainflow counting based fatigue damage for 6-Feb-01 where there is a significant variation of epsilon over the 7 hours and 40 minutes presented. There is a clear match between epsilon (and standard deviation as also shown in Fig. 6a) and fatigue damage computed using either an epsilon based formulation or a rainflow counting approach. Consistancy of the two fatigue assessment methods is evident from the correlation plot shown in Fig 17 (a). The DnV F3 class fatigue curve ($N \leq 10^6$ cycles, $m_1 = 3$) was used. This is defined as:

$$Log(N) = Log(\bar{a}_1) - m_1 \; Log(S) \tag{19}$$

Bending stresses were calculated based on curvature measurements of the monitoring rod inserted in the hydraulic control hose of the umbilical, with stress reference to an outer armour wire.

$$BS = E \frac{d_{wire}}{2} \kappa \tag{20}$$

With:

E : Young's modulus in the case of an umbilical is considered as that of the steel armour layers.

d_{wire} : armour wire radial thickness

κ : monitoring rod curvature (1/m)

Mean stresses including components from tensile stresses owing to tension were not taken into account. A more detailed fatigue analysis could account for these if required by appropriate modification of the chosen S-N curve. This might also preferably account for varying skewness., although it is not expected that the effect would be particularly significant in the case of the umbilical considered herein.

4.6.3 Comparison of fatigue damage owing to mooring, waves, and VIV

The same approach presented for VIV was applied in the mooring and wave frequency ranges. Figs 14, 15, and 16, present the global fatigue damage assessment of the Foinaven umbilical for a selected period (again 6-Feb-01) taking into account the contribution of VIV, wave excitation, and mooring response. The frequency ranges considered are shown in Table 1.

Both fatigue estimation methods (epsilon and rainflow counting) appear to be well-correlated in the VIV and wave ranges (Fig. 17 (a), (b)). The correlation is poor in the mooring case (Fig 17 (c)). This is not surprising since there are very few cycles recorded for these very low mooring system frequencies in each data record, and so the calculation of epsilon and standard deviation is restricted.

In the wave frequency range, as expected, curvature tends to be very narrow-banded as shown by the scatter of 1-epsilon value of around 0.70 (i.e. low values of epsilon).

Fig. 18 presents a comparison of the relative contribution of VIV, wave, and mooring frequency responses to fatigue damage using both methods. For this segment, wave frequency bending stress response (either directly by waves or vessel wave induced motion) appears to be the predominant source of fatigue for the umbilical. VIV can account for a significant part when the regime of vibration becomes narrow-banded as shown on Fig. 18 for records 43 to 53. According to the Rainflow means of fatigue assessment the VIV contribution to damage in this range is seen to exceed that induced by wave/vessel motion (whereas for the epsilon-based fatigue assessment based upon Wirsching and Light's approach it is not).

5. Conclusions

For marine usage the bandwidth parameter epsilon was originally proposed by Cartwright and Longuet-Higgins in 1956 to investigate the distribution of wave heights. The epsilon parameter based on a peak counting approach has been successfully applied to assess the bandwidth variations of the curvature response of a subsea umbilical in particular for VIV. Epsilon exhibits a scatter of values between 0 and 1 and enables rapid assessment of the VIV bandwidth regime with time (usefully over periods of hours as well as days). The use of the epsilon method indicates that vortex induced vibrations may build up

gradually (in terms of amplitude) with associated narrowing of bandwidth as a consequence of varying current for the particular umbilical examined and it is likely to most other similar configurations.

Analysis of the peaks of power spectral density of curvature has shown with the help of epsilon that in general as VIV amplitude response increases around the predominant frequency as its bandwidth narrows (with increasing current). It is seen that this frequency also varies by a small amount in the same sense as the current speed. The strong match between current speed and standard deviation of curvature implies that the lack or unavailability of current data could be approximated knowing the curvature response of the umbilical when predicting the level of VIV that the structure is likely to experience.

The influence of the current speed has demonstrated in some instances consistent multiple distinct peak frequencies being excited (although a single peak still predominates). These forms of behaviour correspond to characteristics which have been demonstrated by a number of VIV prediction tools, including that (VIVALL) developed by the authors (although not presented here). Our improving understanding of the behaviour of the bandwidth of VIV in the type of structure investigated here increases our confidence in being able to make fatigue assessments by the use of the response characteristics introduced here.

Some results showing the relative contributions of VIV and waves/vessel motions indicate instances when the VIV contribution to fatigue is proportionately significant (at high current speeds). Other fatigue assessment models based on epsilon are currently being investigated and developed by the authors which are expected to improve on the Wirsching and Light approach when applied to VIV.

Although epsilon was applied to measured curvature data in this study, it is possible to implement this bandwidth parameter on predicted curvature data at a design stage. This can be achieved using a VIV prediction model such as VIVALL. A time-domain simulation module within VIVALL enables to generate curvature time-series at different locations along the structure owing to given wave, vessel motion and current profile combinations. It is then possible to implement the epsilon calculation as a basis for different fatigue models such as Wirsching & Light.

Whilst only the X component of response has been presented here, full analysis requires that the same procedure for the Y component be performed. The contribution to fatigue damage owing to each component remains an issue linked to the complex problem of 3D VIV excitation and response where improvement in understanding of the interaction between the X and Y components along the length of risers and umbilicals is required.

As a final conclusion, the value of the epsilon parameter is threefold:

- Give a useful insight of the variations of bandwidth on measured or predicted time-series therefore of changes of VIV regime that the structure is experiencing in a given combination of wave, vessel motion and current profile.
- Enable a fatigue damage assessment of subsea risers and umbilicals owing to VIV which is to date, poorly understood and referenced.

- Provide a relatively "simple" measure to implement on large data sets such as gathered by a 24/7 monitoring unit like the Foinaven Umbilical Monitoring System operating remotely with limited possible technical intervention.

The future offers the promise of more detailed monitoring capabilities such that these issues may be better understood even if not entirely resolved.

Acknowledgements

The authors wish to acknowledge the assistance of BP for providing access to the FUMS data, Fugro GEOS for the current data, staff at BPP Technical Services, and Dr K R Drake (UCL) for their technical support.

References

Barltrop N. D. P. and Adams A. J., Dynamics of Fixed Marine Structures, publ Butterworth-Heinemann, ISBN 0750610468, 1991.

BPP Technical Services Ltd., Analysis of umbilical performance on the FPSO Foinaven Petrojarl, measurement period 16-Jun-00 to 12-Jul-00, Report ref : TS95/0202 Re: (14) 2/00, 2000.

BPP Technical Services Ltd., Analysis of umbilical performance on the FPSO Foinaven Petrojarl, measurement period 25-Jan-01 to 13-May-01, Report ref : TS95/0202 Re: (17) 1/01, 2001.

Cartwright D. E. and Longuet-Higgins M. S., The statistical distribution of the maxima of a random function, Proceedings of the Royal Society, A, Vol. 237, pp 212-232, 1956.

Crandall S. H., Mark W. D. and Khabbaz G. R., The variance in Palmgren-Miner damage due to random vibration, Proc. 4th U.S. Natl. Congr. App. Mech., Berkeley, vol. 1, pp 119-125, June 1962.

Fang J. and Lyons G. J., Application of a general prediction method for vortex induced vibrations of catenary risers', ISOPE, Proc 1st International Offshore and Polar Engineering Conference, Edinburgh, ISBN 0-9626104-8-8 (Vol III), pp 354-361, 1991.

Lalane C., Mechanical Vibration and Shock - Fatigue Damage, Vol IV, publ Hermes Penton Science, ISBN 1 9039 96006 6, 2002.

Lin Y. K., Probabilistic Theory of Structural Dynamics, Mc Graw-Hill Book Co., 1967.

Longuet-Higgins M. S., On the statistical distribution of the heights of sea waves, Journal of Marine Research, vol. XI, number 3, pp 245-266, 1952.

Lyons G. J. and Patel M. H., A prediction technique for vortex induced transverse response of marine risers and tethers, J. Sound and Vibration, vol. 111, pp 467-487, 1986a.

Lyons G. J., On the hydrodynamics of tensioned slender flexible cylinders, PhD Thesis, University of London, 252 pages, 1986b.

Lyons G. J., Brown D. T., Cook H. H., Walls B. and Barnay G., The Foinaven Umbilical Performance Monitoring System – A New Approach, Proceedings of the Offshore Technology Conference, OTC 8883, 1998.

Lyons G. J., Vandiver J. K., Larsen C. M. and Ashcombe G. T., Vortex induced vibrations measured in service in the Foinaven dynamic umbilical, and lessons from prediction, Journal of Fluids and Structures, 17(8), 2003.

Mandal S., Witz J. A., and Lyons G J., Reduced order ARMA spectral estimation of ocean waves', Applied Ocean Research, Vol 14 No 5 pp 303-312, 1992.

Matsuishi M., Endo T., Fatigue of metals subjected to varying stress, presented at the Japan Society of Mechanical Engineers, Fukuoka, Japan, 1968.

Miles J. W., On structural fatigue under random loading, Journal of Aeronautical Science, no. 21 pp 753-762, 1954.

Rice S. O., Mathematical analysis of random noise, Bell System Technical Journal, no. 23 vol. 282, 1944.

Rice S. O., Bell System Technical Journal, no. 24, vol. 46, 1945.

Trarieux F. and Lyons G. J., Novel use of a bandwidth measure for vortex induced vibrations – Case Study: The Foinaven umbilical, Fluid Structure Interaction Symposium, IUTAM, New Brunswick, NJ, USA, 2003.

Trarieux F. and Lyons G. J., Detailed analysis of the vortex induced vibration (VIV) frequency content of the Foinaven umbilical, Flow Induced Vibration 2004 (FIV2004) Conference, Paris, France, 2004.

Trarieux F., An investigation of vortex induced vibrations of subsea risers and umbilicals from offshore field measurements, PhD thesis, University of London, 2004.

Trarieux F. and Lyons G. J., Fatigue damage assessment using a bandwidth parameter for VIV applied to the Foinaven dynamic umbilical, 24th International Offshore Mechanics and Arctic Engineering Conference, OMAE2005-67024, Halkidiki, Greece, 12-17 June 2005.

Tucker M. Carter D. and Challenor, P. Numerical simulation of a random sea: a common error and its effect upon wave group statistics. Applied Ocean Research, Vol. 6, No. 2, pp 118-122, Apr 1984.

Det norske Veritas, Offshore Standard – Dynamic Risers, DNV-OS-F20, Appendix B, pp 70-71, January 2001.

Vandiver J. Predicting lock-in on drilling risers in sheared flows, Proceedings of the 7th Flow Induced Vibration Conference 2000, Lucerne, Switzerland, 2000.

Wirsching P and Light M, Fatigue under wide band random process, Journal of the Structural Division, vol. 106, no. ST7, pp 1593-1607, July 1980.

Yu L, Das and P, Barltrop N, A new look at the effect of bandwidth and non-normality on fatigue damage, Fatigue Fracture Engineering Material Structures, vol. 27, pp 51-58, 2004.

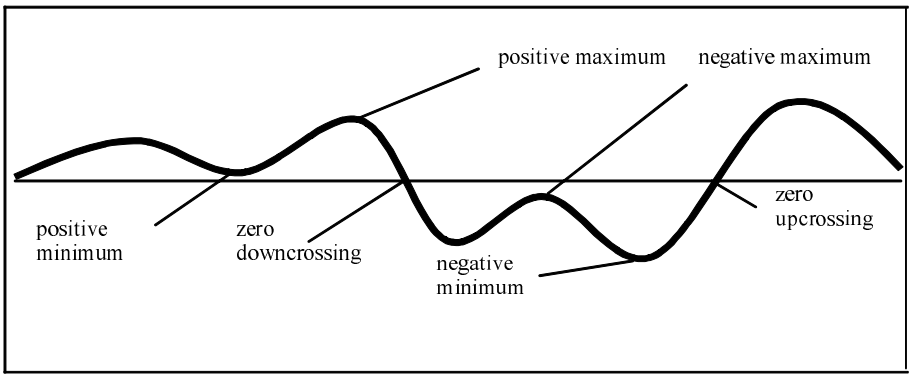

Figure 1. Some signal definitions

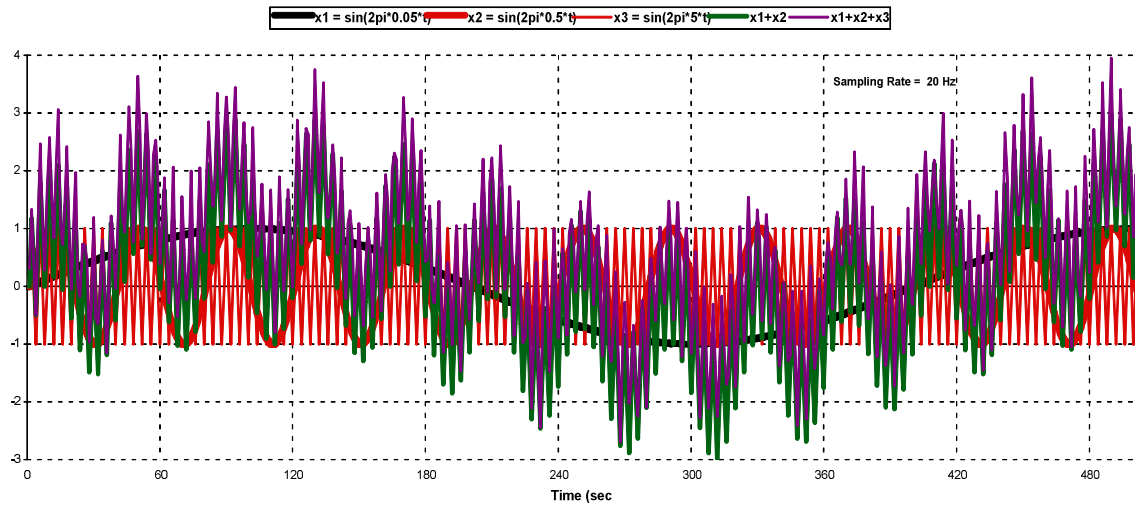

Figure 2. Negative maxima as a proportion of total maxima for sum of 3 sinusoids

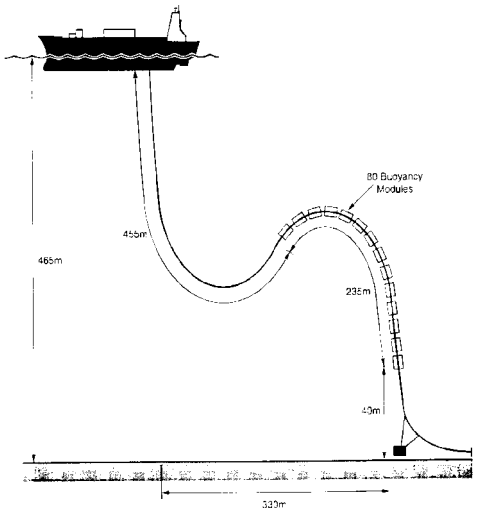

Figure 3. Foinaven umbilical configuration

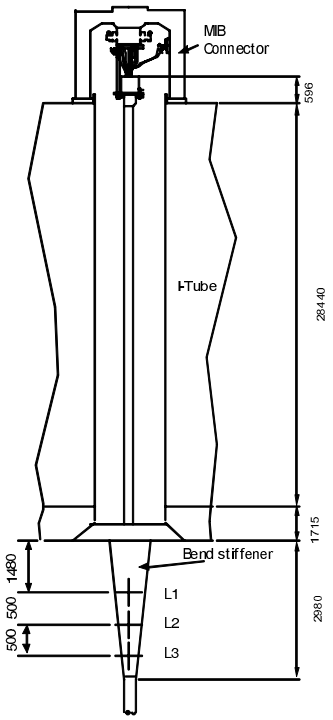

Figure 4. Umbilical exit from turret showing location of 3 curvature sensing locations L1, L2, and L3

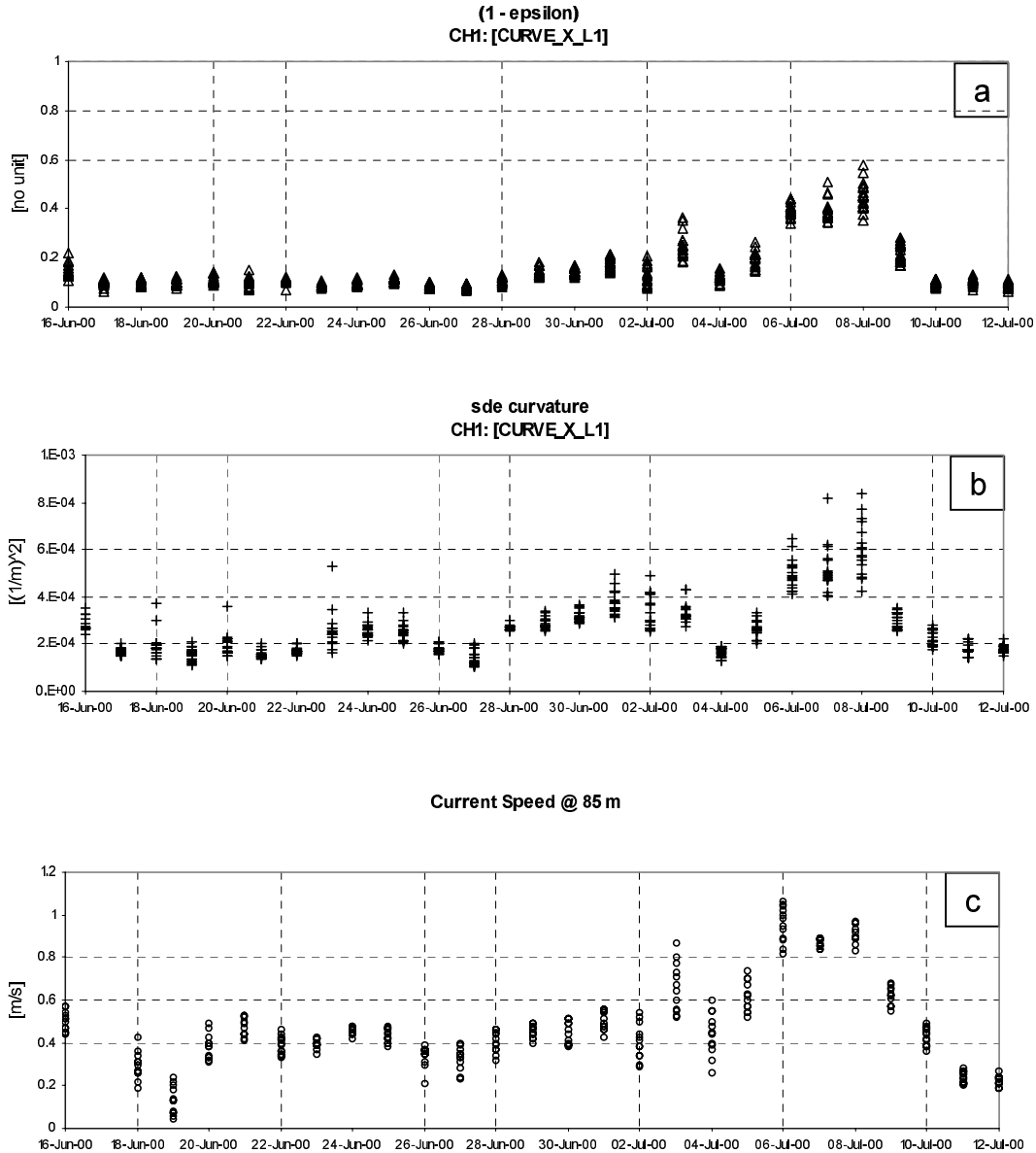

Figure 5a.

Comparison of epsilon with standard deviation, kurtosis, and current speed (at 85 m). Channel 1 (X component of curvature at sensor location L1), data 16 June to 12 July 2000 (VIV Filter 0.2 to 2 Hz). a: 1-epsilon (grouped); b: standard deviation (grouped); c: current speed (grouped);

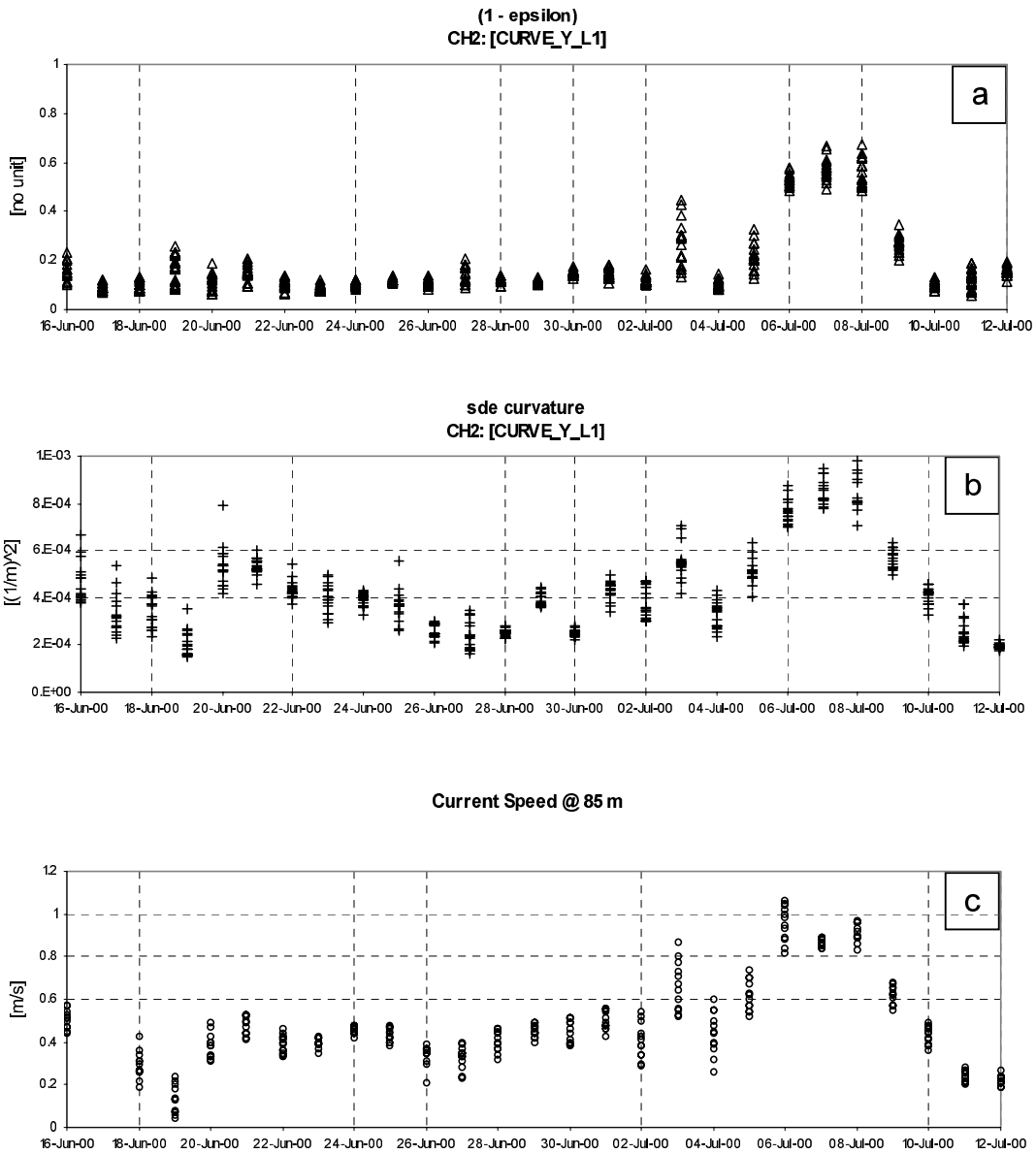

Figure 5b.

Comparison of epsilon with standard deviation, kurtosis, and current speed (at 85 m). Channel 2 (Y component of curvature at sensor location L1), data 16 June to 12 July 2000 (VIV Filter 0.2 to 2 Hz). a: 1-epsilon (grouped); b: standard deviation (grouped); c: current speed (grouped);

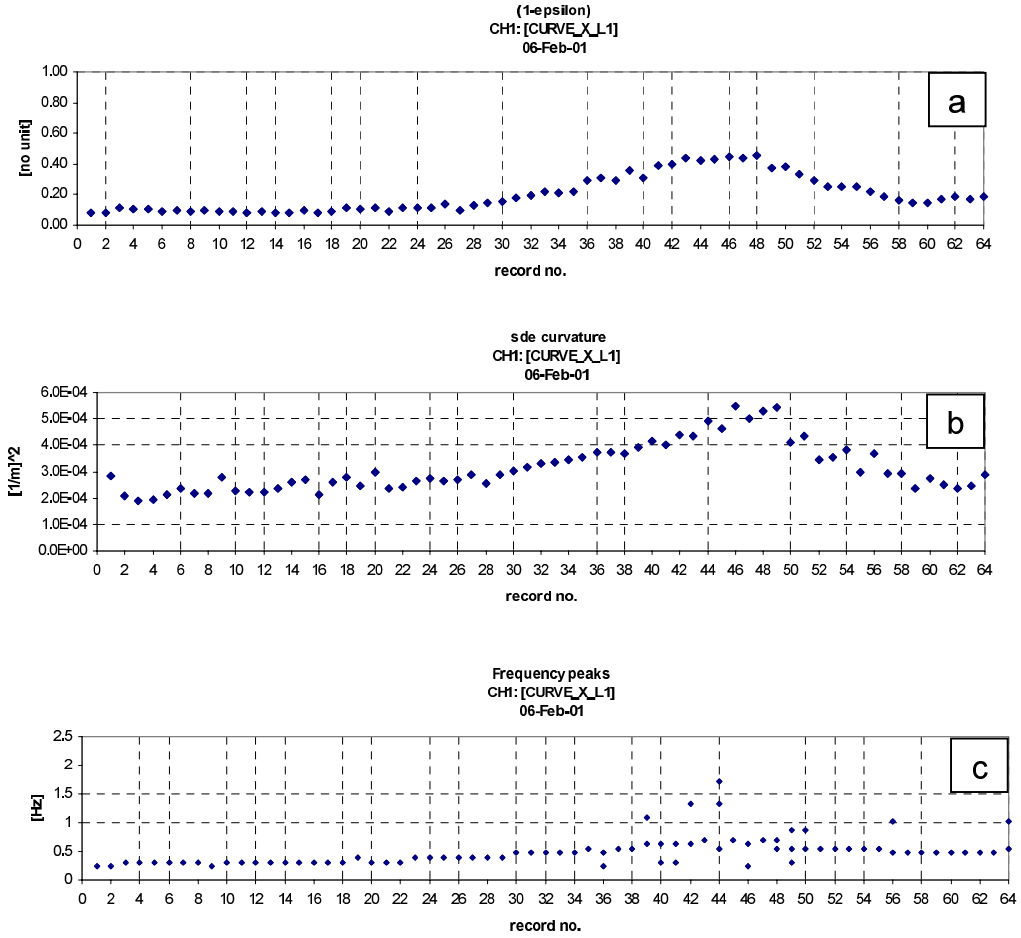

Figure 6a.

Daily variation (00h00-07h40) / 64 records:
a: (1-epsilon); b: sde curvature; c: frequency peaks

XL1 component

06-Feb-01

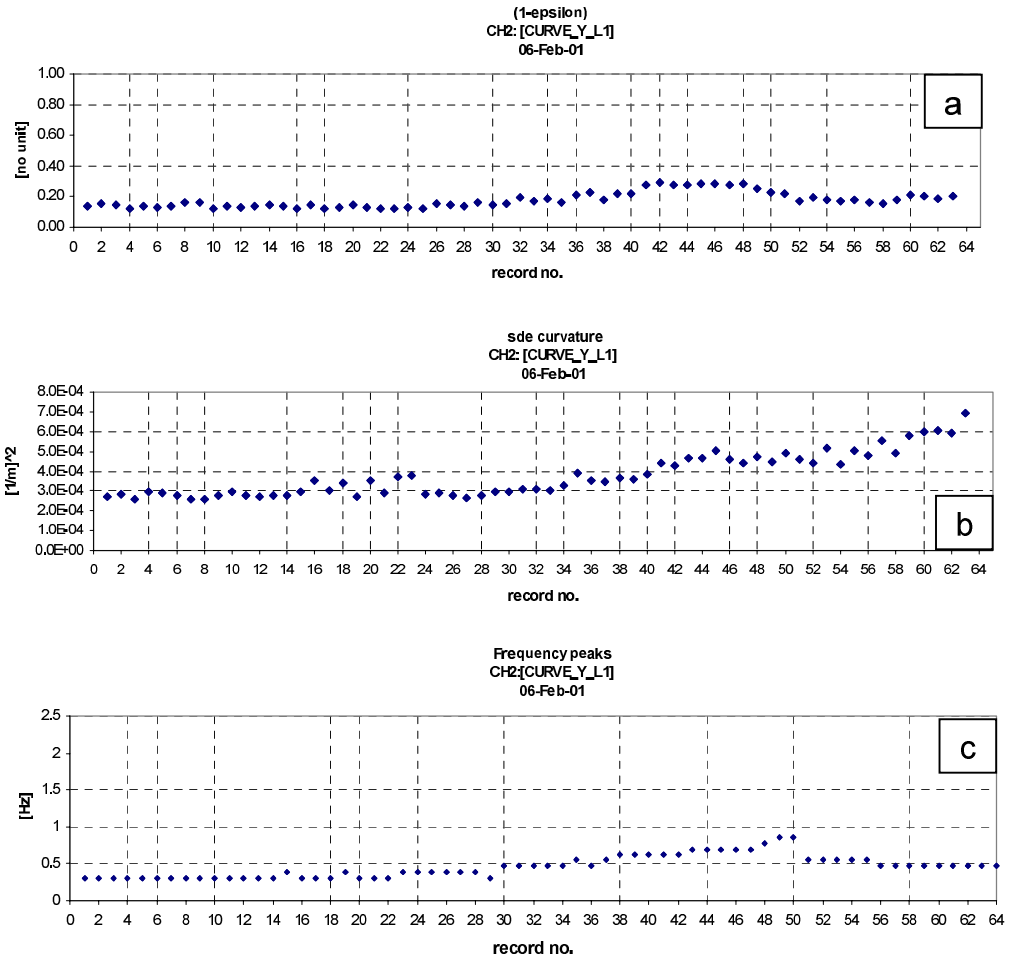

Figure 6b.

Daily variation (00h00-07h40) / 64 records:
a: (1-epsilon); b: sde curvature; c: frequency peaks

YL1 component

06-Feb-01

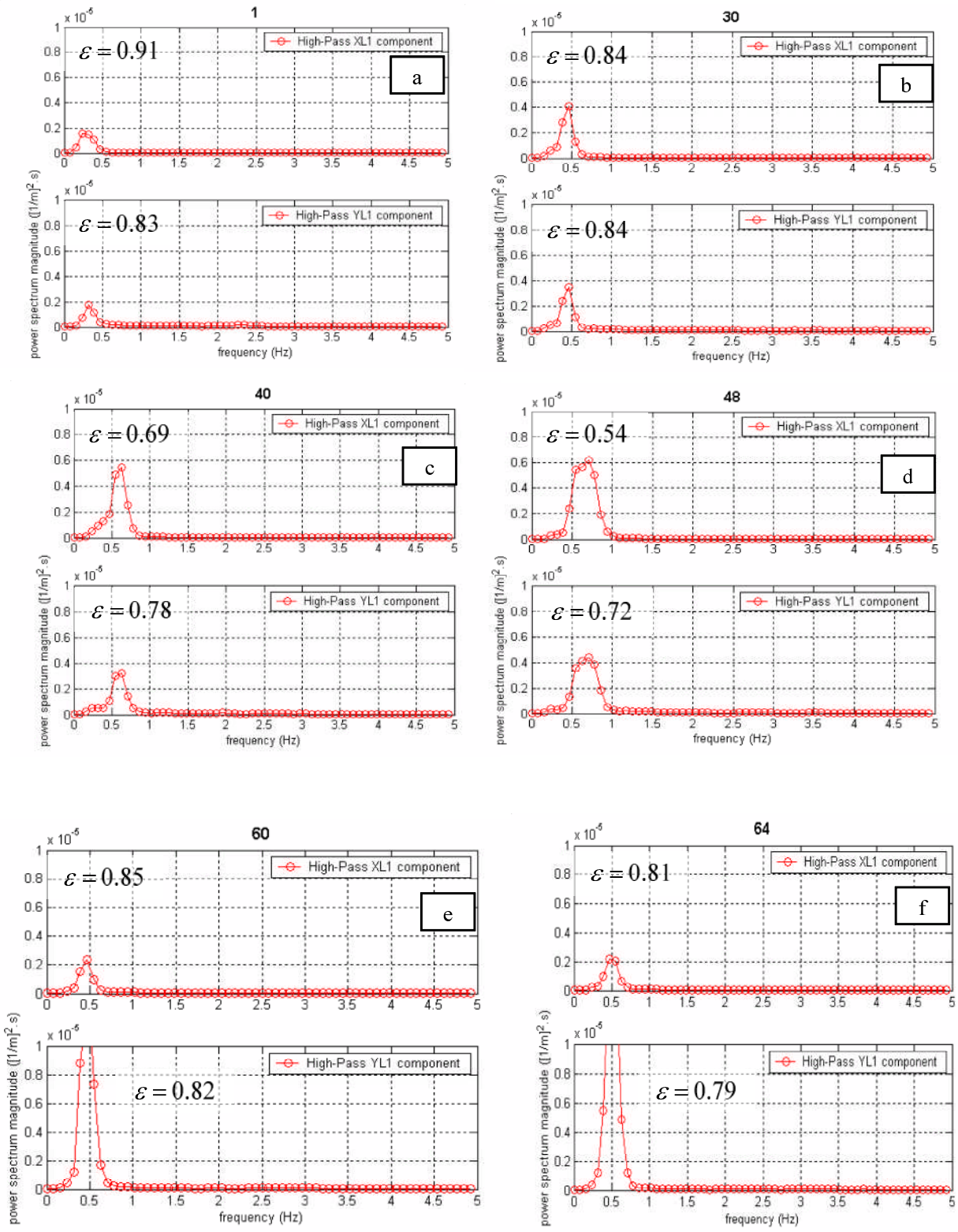

Figure 7
Variation of amplitude of power spectral density of curvature / 06-Feb-01;
a: record no. 1; b: record no. 30; c: record no. 40; d: record no. 48; e: record no. 60; f: record no. 64

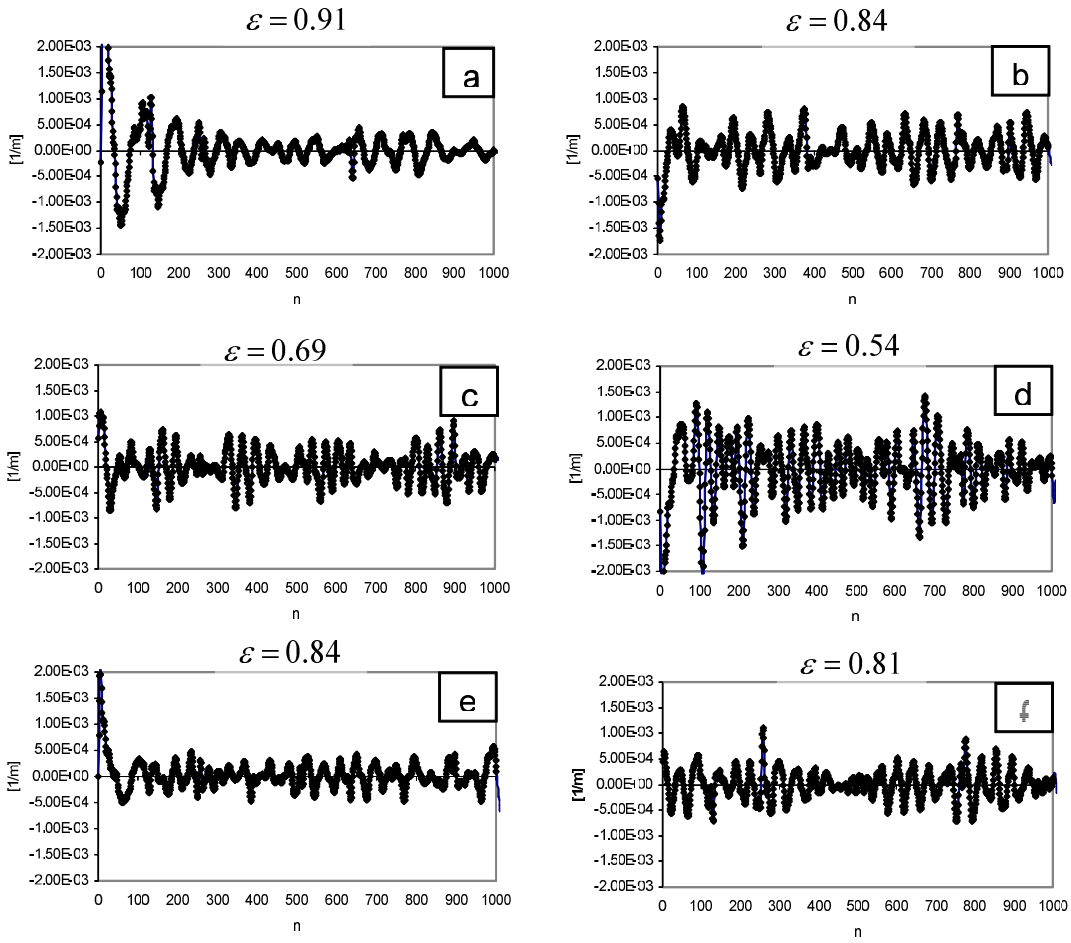

Figure 8
Filtered curvature signal – XL1 component
06-Feb-01
a: record no. 1; b: rec. 30; c: rec. 40; d: rec. 48; e: rec. 60; f: rec. 64;

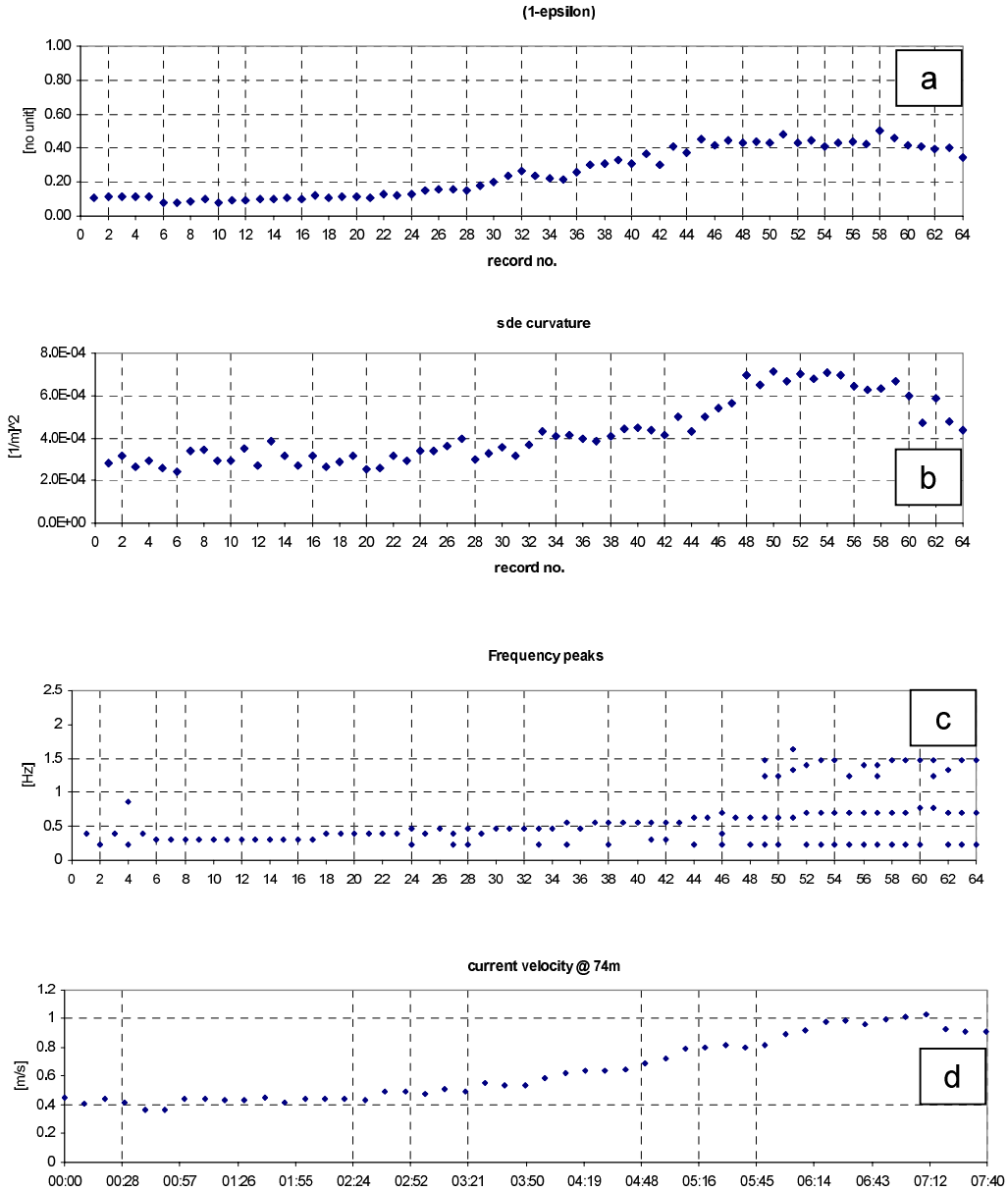

Figure 9a.

Daily variation (00h00-07h40) / 64 records:
a: (1-epsilon); b: sde curvature; c: frequency peaks; d: current speed@ 74m.

XL1 component

20-Feb-01

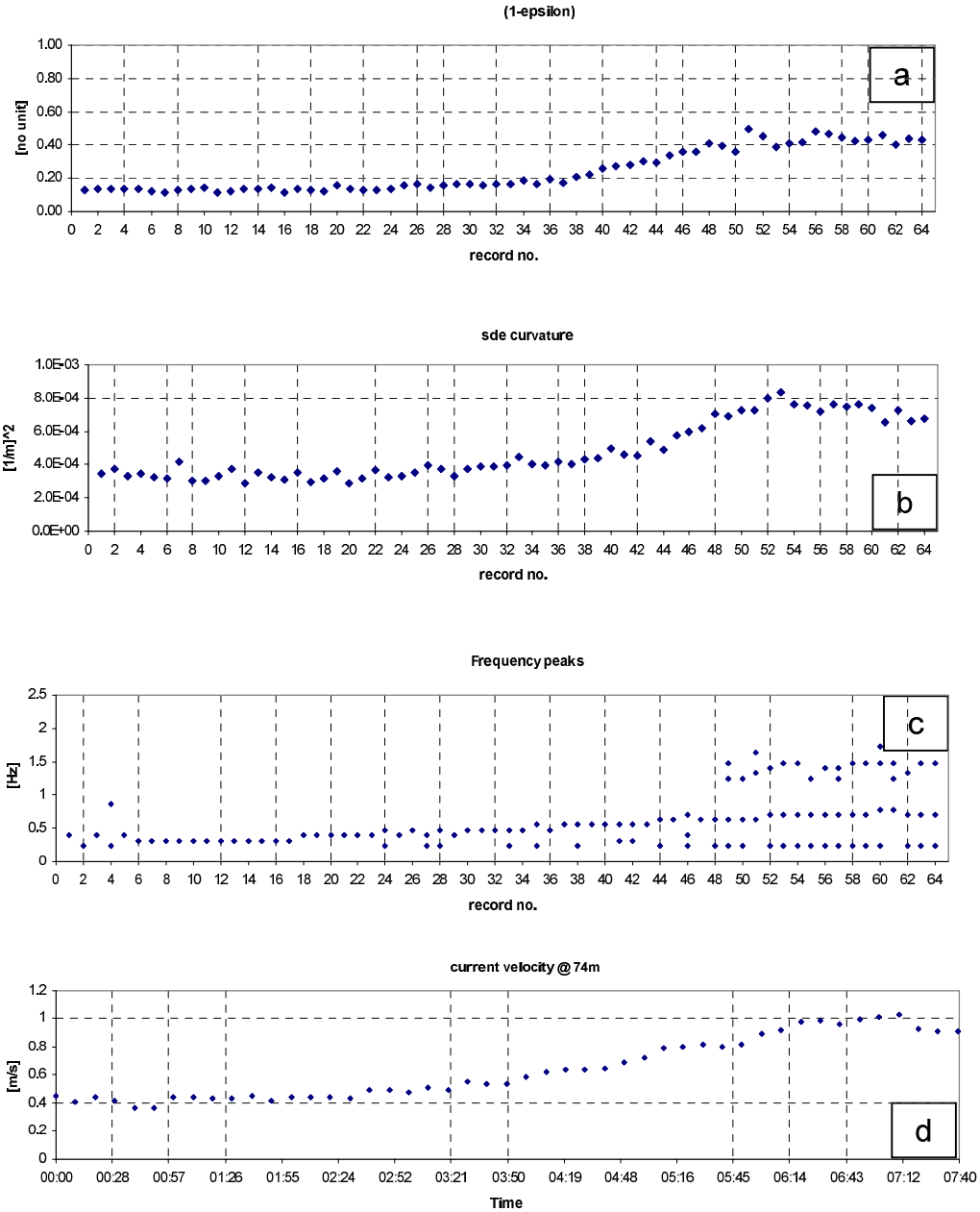

Figure 9b.

Daily variation (00h00-07h40) / 64 records:
a: (1-epsilon); b: sde curvature; c: frequency peaks; d: current speed@ 74m.

YL1 component

20-Feb-01

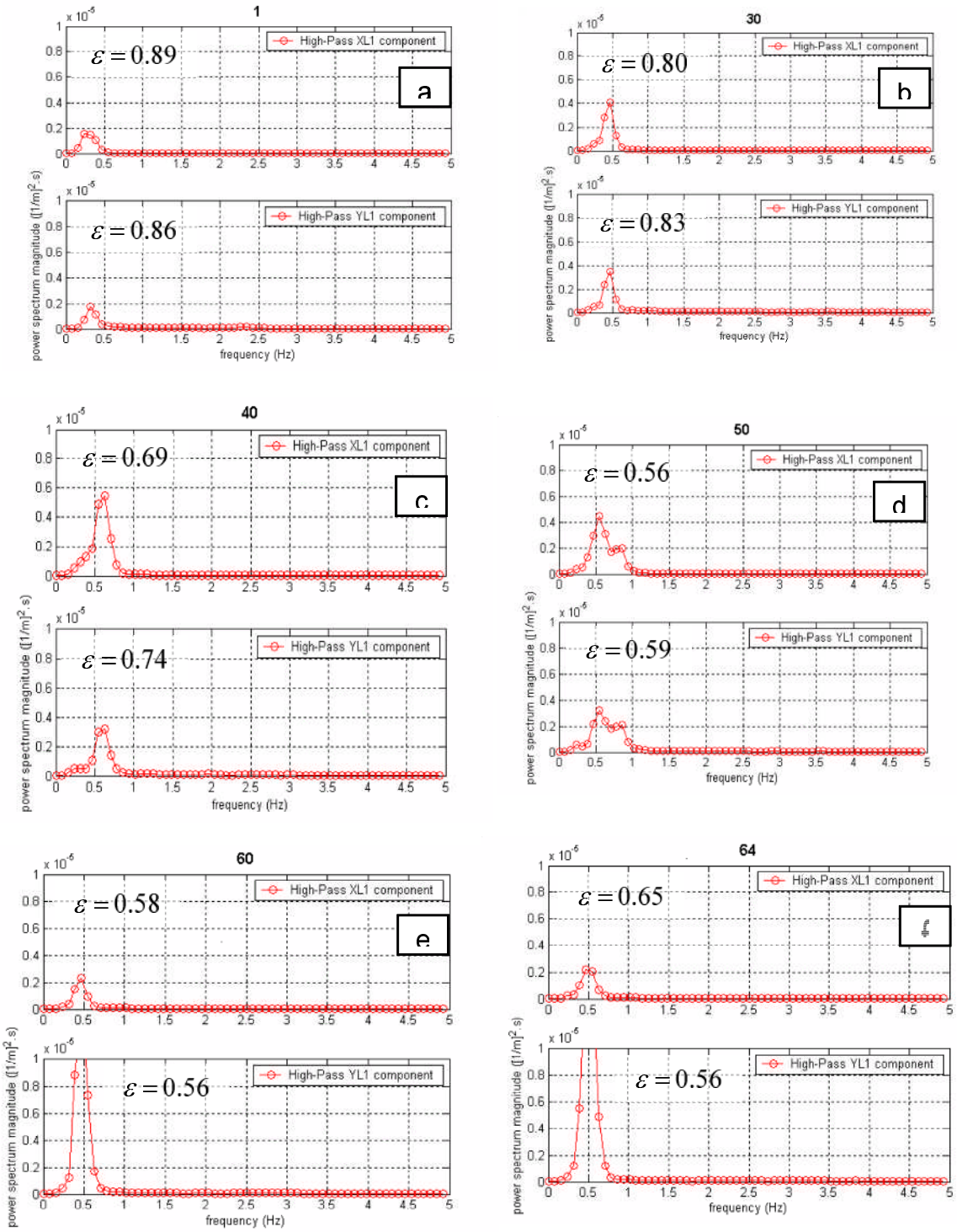

Figure 10.
Variation of amplitude of power spectral density of curvature / 20-Feb-01;
a: record no. 1; b: record no. 30; c: record no. 40; d: record no. 48; e: record no. 60; f: record no. 64

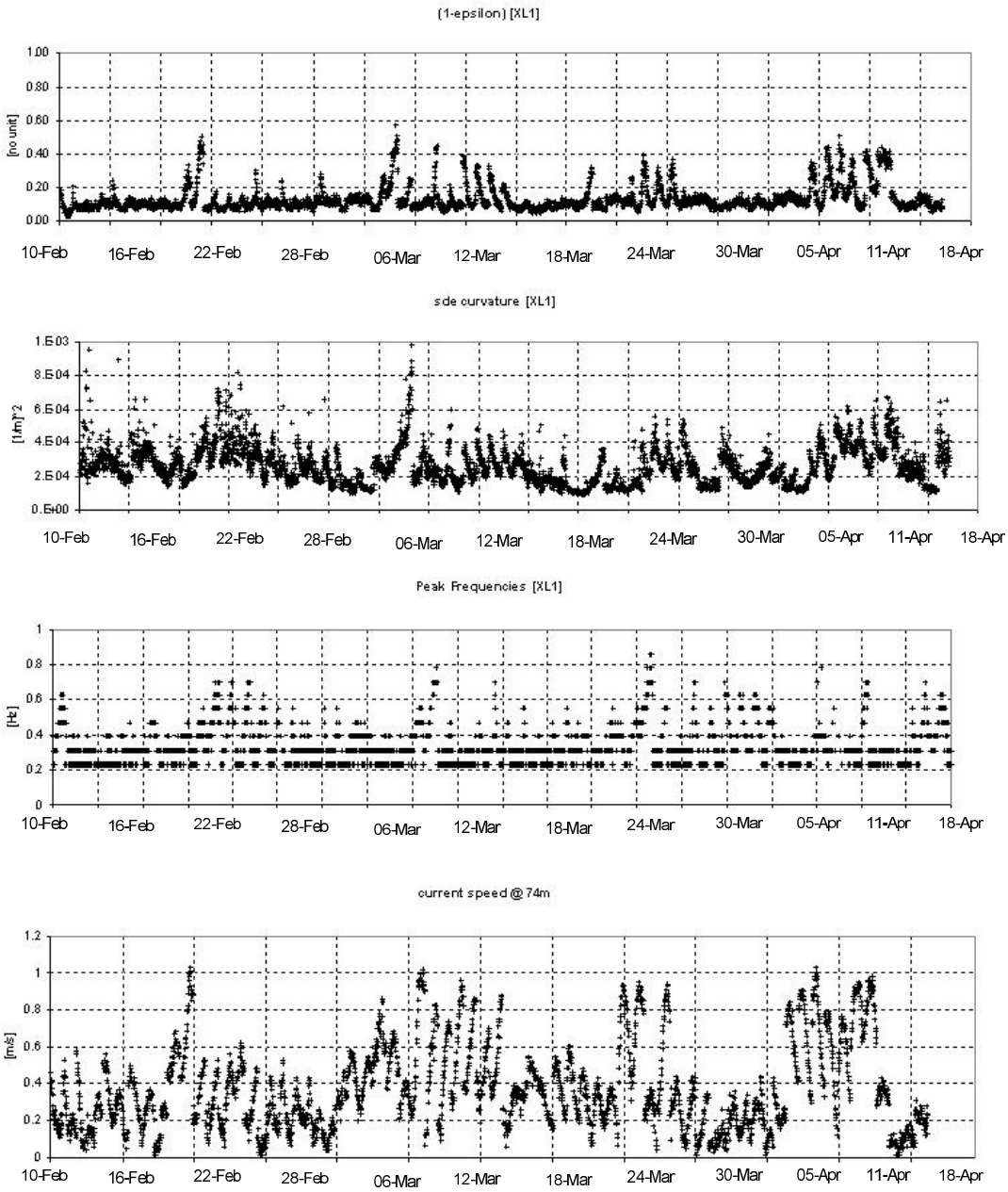

Figure 11.

Variation of epsilon with standard deviation of curvature, peak frequencies and current Channel 1: (X component of curvature at sensor location L1)

a: (1-epsilon); b: sde curvature; c: peak frequencies; d: current speed at 74m

10-Feb-01 / 18-Apr-01

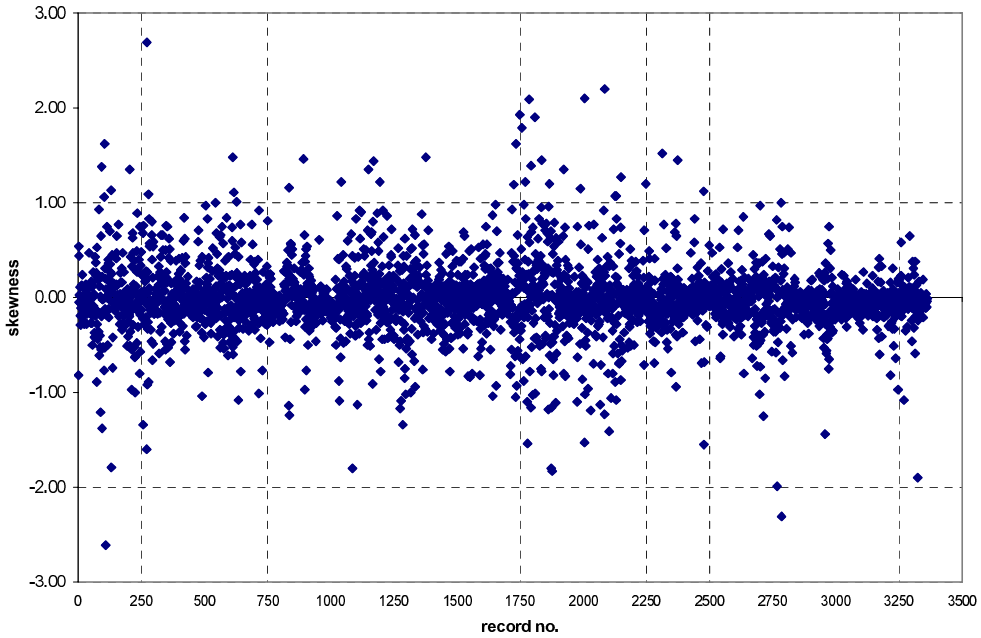

Figure 12 . Variation of Skewness of curvature

CH1: [Curve_X_L1]
25-Jan-01 / 18-Apr-01

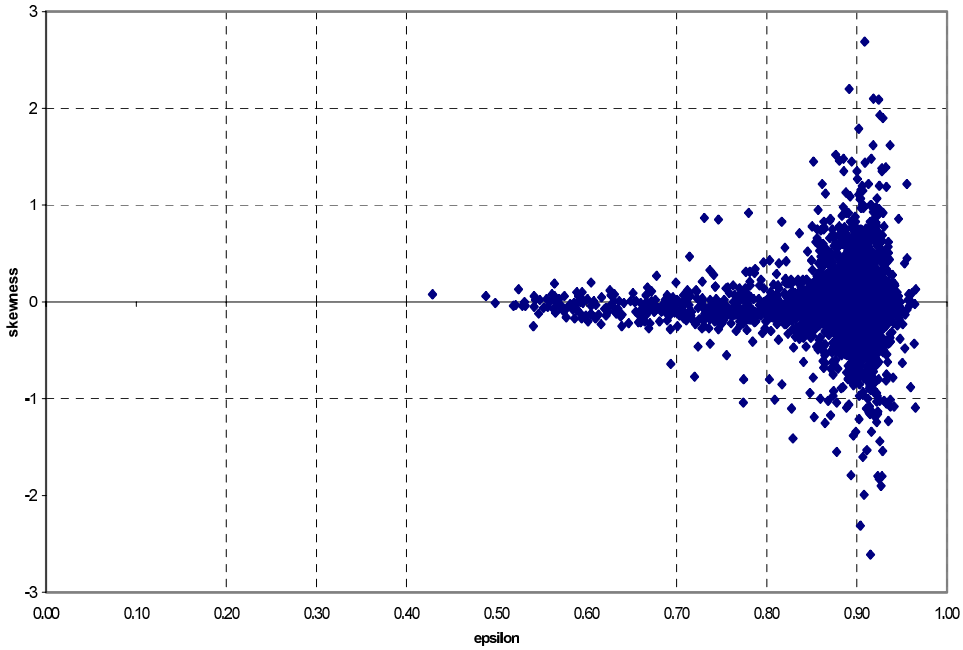

Figure 13. Correlation Skewness with Epsilon

CH1: [Curve_X_L1]
25-Jan-01 / 18-Apr-01

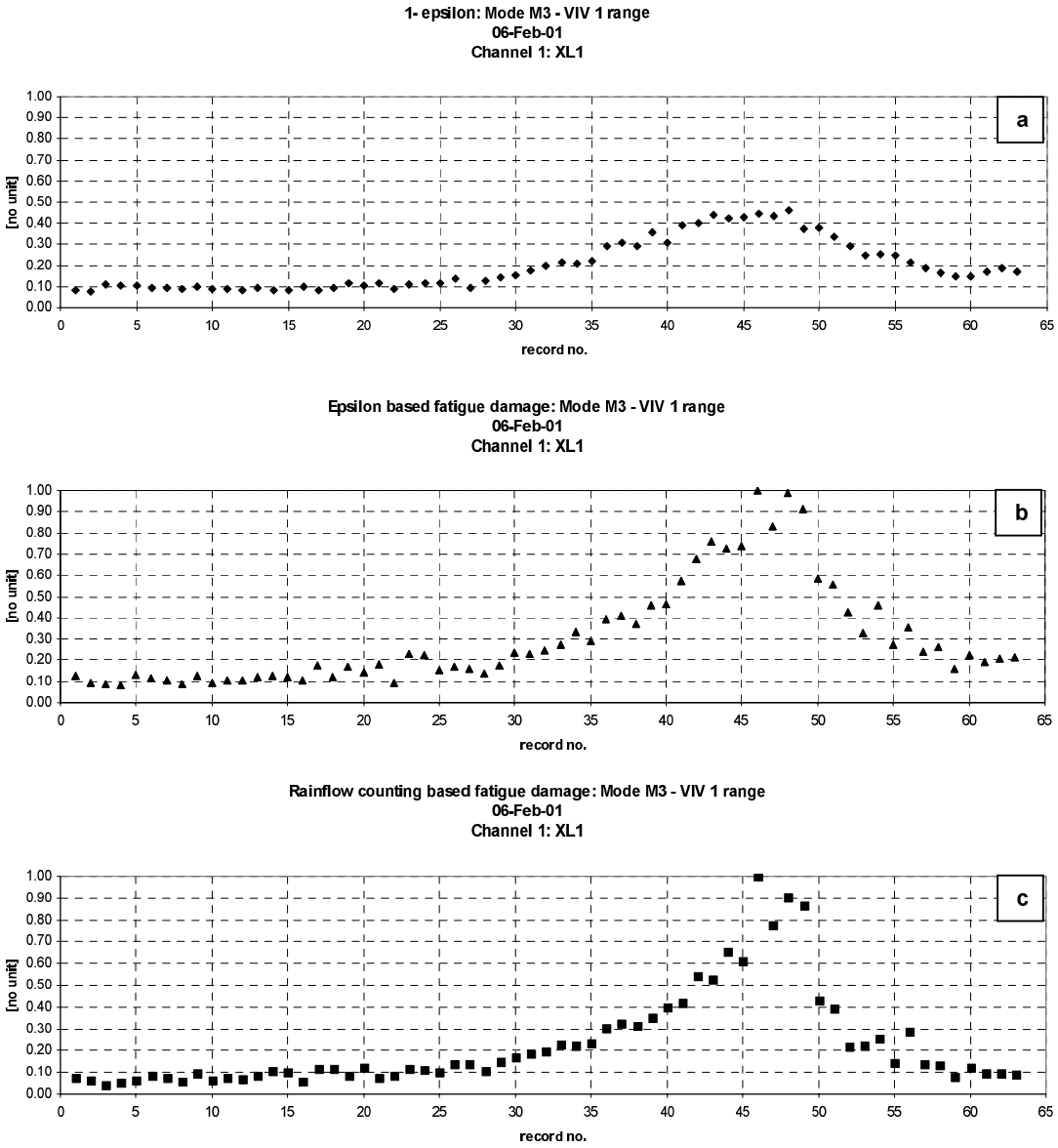

Figure 14.

Daily variation (00h00-07h40) / 64 records:
a: 1- epsilon; b: epsilon based fatigue damage; c: rainflow counting based fatigue damage;

XL1 component – Mode 3 : VIV 1 range : [0.2 – 2 Hz]

06-Feb-01

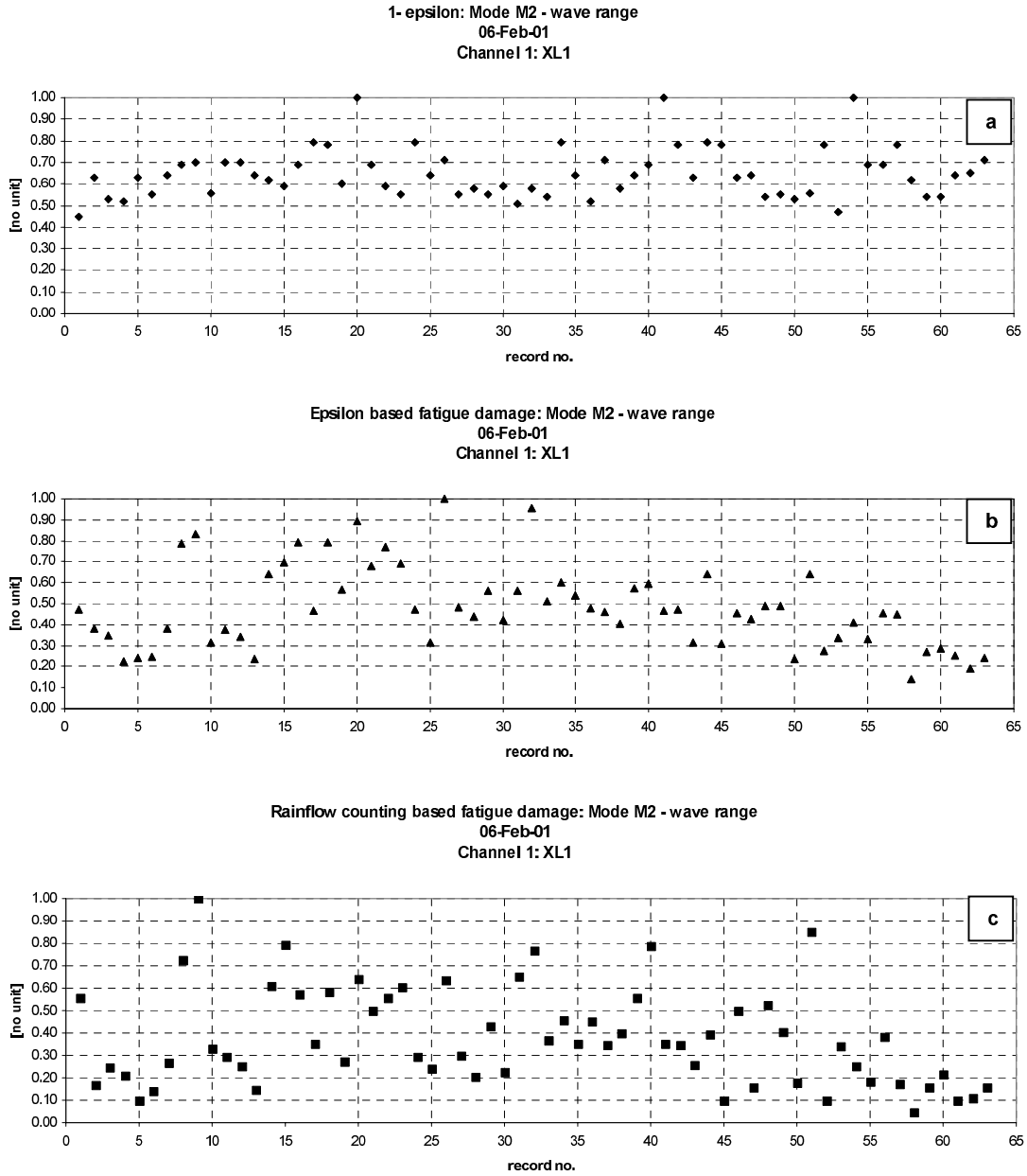

Figure 15.

Daily variation (00h00-07h40) / 64 records:
a: 1- epsilon; b: epsilon based fatigue damage; c: rainflow counting based fatigue damage;

XL1 component – Mode 2 : Wave range : [0.05 – 0.2 Hz]

06-Feb-01

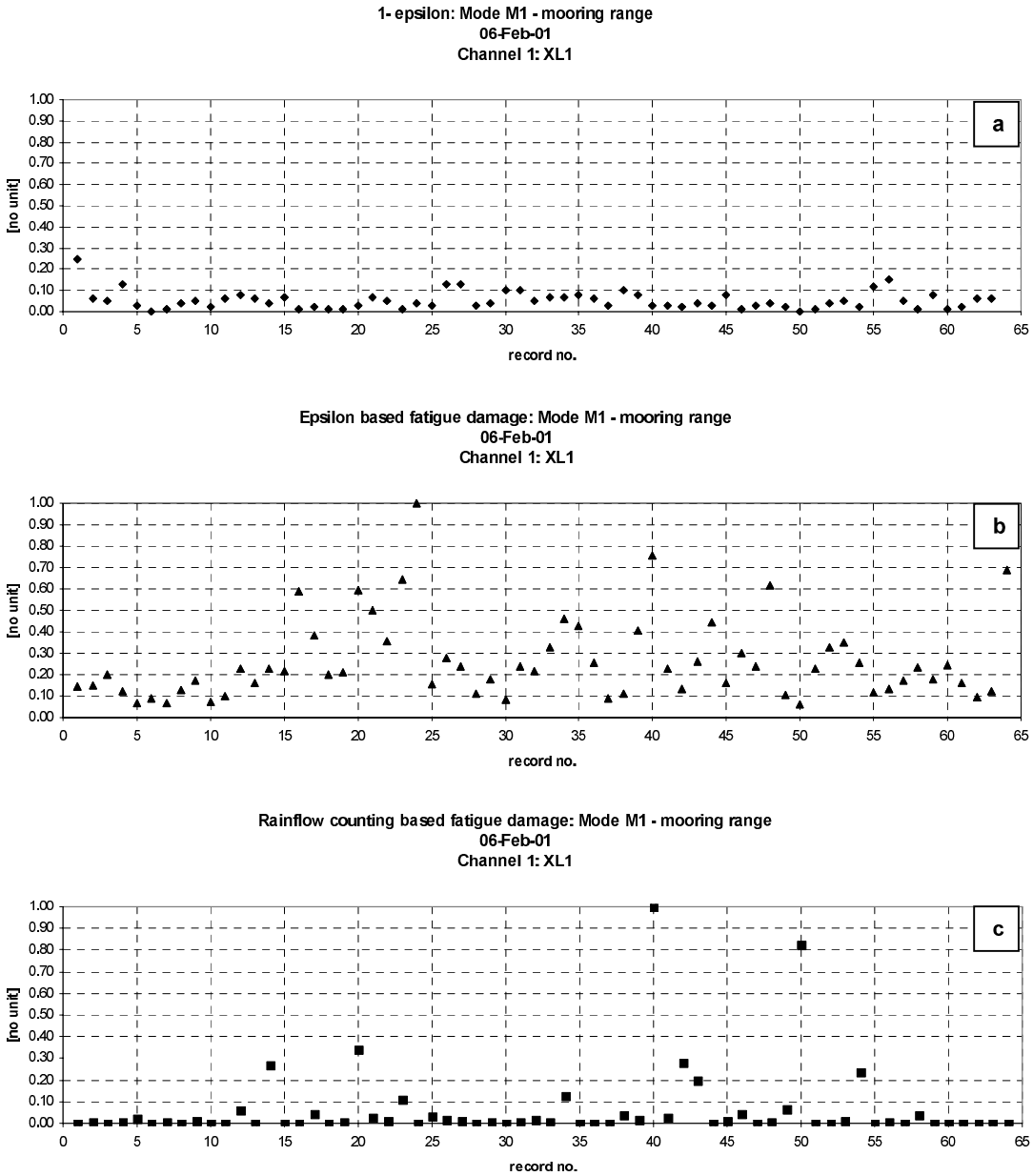

Figure 16.

Daily variation (00h00-07h40) / 64 records:
a: 1- epsilon; b: epsilon based fatigue damage; c: rainflow counting based fatigue damage;

XL1 component – Mode 1 : Mooring range : [0.083 – 0.05 Hz]

06-Feb-01

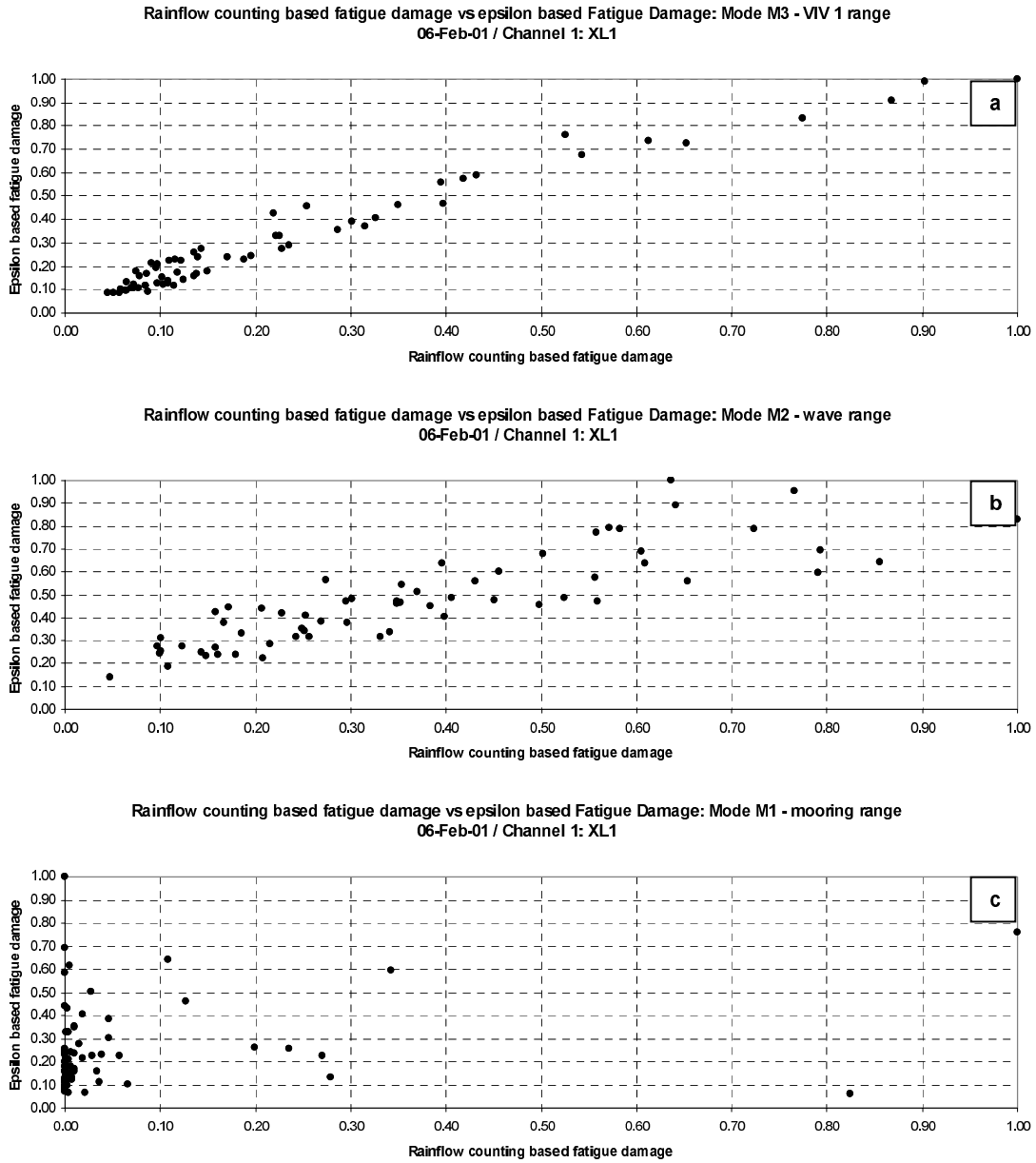

Figure 17.

Daily variation (00h00-07h40) / 64 records:

Rainflow counting vs epsilon based fatigue damage

a: VIV; b: wave; c: mooring;

XL1 component

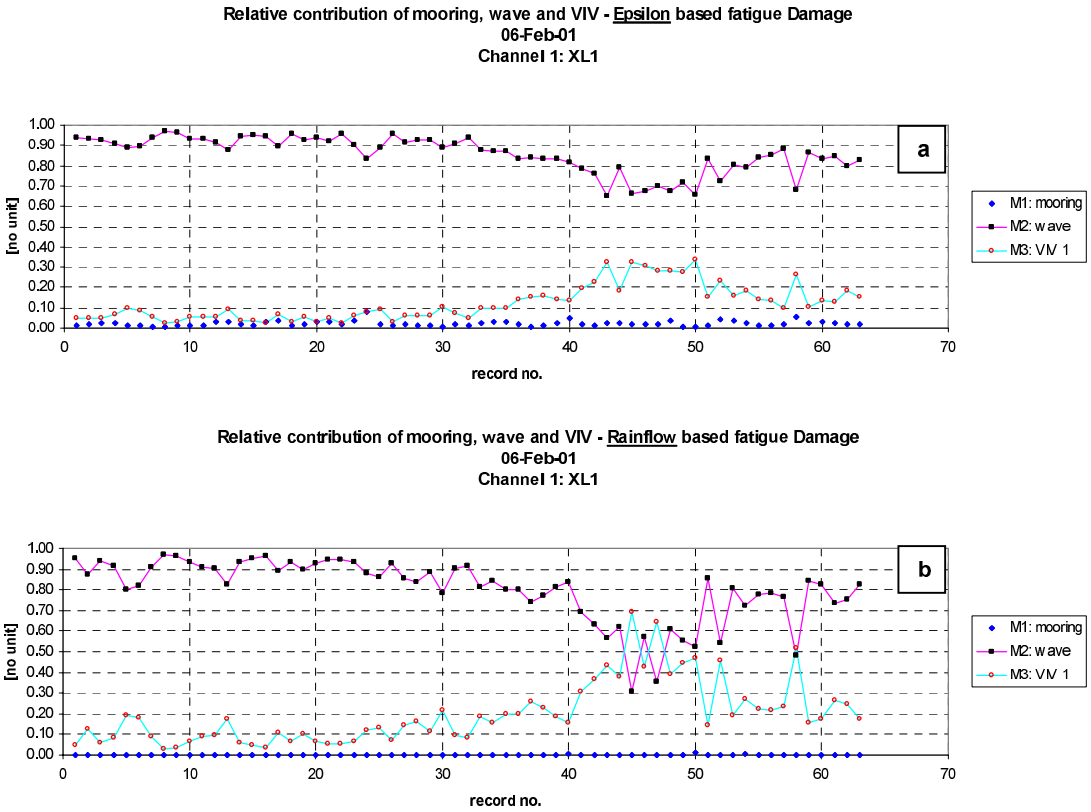

Figure 18.

Relative contribution of mooring, wave and VIV to fatigue damage:

epsilon based (a) & rainflow counting based (b) fatigue damage assessment

XL1 component

06-Feb-01 - Daily variation (00h00-07h40) / 64 records

Band reference	**Type**	**Frequency range (Hz)**	**Period range (seconds)**
M1	Mooring	0.083 – 0.05	20 – 120
M2	Wave	0.05 – 0.2	5 – 20
M3	VIV	0.2 – 2	0.5 – 5

Table 1. Frequency bands